

Fabry-Perot Bragg Grating Nanoresonator with Ultrahigh Intrinsic Q Based on Low-loss Silicon Nitride

YANG ZHANG¹, SYLVAIN VEILLEUX², AND MARIO DAGENAIS^{1,*}

¹*Department of Electrical and Computer Engineering, University of Maryland, College Park, MD 20742, USA*

²*Department of Astronomy, University of Maryland, College Park, MD 20742, USA*

**dage@umd.edu*

Abstract: Photonic integrated circuits based on ultralow loss silicon nitride waveguides have shown significant promise for realizing high-performance optical systems in a compact and scalable form factor. For the first time, we have developed a Fabry-Perot Bragg grating nanoresonator based on silicon nitride on silicon dioxide platform with an ultra-high intrinsic quality factor of 19.3 million. By combining the introduction of tapered grating between cavity and periodic Bragg grating, increasing the width of cavity to multi-mode region and optimized annealing strategy for Si₃N₄ film, the propagation loss is reduced to around 0.014 dB/cm. Fabry-Perot Bragg grating nanoresonator can be easily implemented in a simple straight waveguide occupying a minimal amount of space. Therefore, it is a key component to build a high performance photonic integrated circuit for many applications.

© 2023 Optica Publishing Group under the terms of the [Optica Publishing Group Open Access Publishing Agreement](#)

1. Introduction

In the past decade, photonic integrated circuits (PICs) have emerged as a promising technology for realizing high-performance optical systems in a compact and scalable form factor. Unlike traditional discrete optical components, which require extensive alignment and assembly, PICs enable the integration of multiple optical functions on a single chip, resulting in reduced size, weight, power consumption, and cost.

The key building blocks of a PIC typically include waveguides, couplers, filters, modulators, detectors, and amplifiers, which can be fabricated using various materials and technologies, such as silicon, silicon nitride, indium phosphide, gallium arsenide, and lithium niobate. The choice of material and technology depends on the specific requirements of the PIC, such as the operating wavelength, bandwidth, polarization, and temperature range, as well as the manufacturing process and cost. Among them, the silicon nitride (Si₃N₄) platform offers a unique combination of low loss, high nonlinearity, large mode area, and CMOS compatibility, making them well-suited for a wide range of applications in optical communications, sensing, computing, quantum optics, and astrophotonics. The key advantage of Si₃N₄ waveguides is their exceptionally low propagation loss, which can be less than 1 dB m⁻¹ [1–3], depending on the waveguide dimensions and fabrication process. This is orders of magnitude lower than the losses of traditional waveguides based on silicon on insulator (SOI), and enables high-quality-factor resonators [1,4,5], long-distance delays, and low-threshold nonlinear effects [6–8]. Moreover, Si₃N₄ waveguides exhibit low polarization-dependent loss, high thermal stability, and compatibility with standard CMOS fabrication processes, making them highly attractive for integration with electronics and other optical components.

Despite these advancements, several challenges remain in the design, fabrication, and integration of Si₃N₄-based PICs, such as the optimization of the waveguide dimensions and

45 materials to achieve the desired performance, the mitigation of fabrication imperfections and
 46 variations, and the integration with other optical and electronic components. In our work, an
 47 ultrahigh quality factor Q_{int} of 19.3 million based on a Fabry-Perot Bragg grating (FPBG)
 48 nanoresonator is demonstrated for the first time. Using an efficient approach based on
 49 measuring the transmission of on-chip Fabry-Perot cavities with various lengths [9,10], we
 50 have extracted the loss of 0.014 dB/cm in our Si_3N_4 film. Compared to the waveguide-coupled
 51 ring resonators, Fabry-Perot Bragg gratings require less engineering in the coupling region and
 52 have no bending losses. This structure is particularly suitable for producing high Q resonators
 53 in the low-confinement Si_3N_4 waveguide platform.

54 The paper is organized as follows. In the following section, we will first briefly discuss the
 55 theory and design for the high-Q FPBG. In Section 3, we will provide the details of the
 56 fabrication process of the device, the measurement set-up, and the experimental results. The
 57 performance of fabricated devices will be analyzed in Section 4. Finally, the outlook towards
 58 future development and conclusions will be given in Section 5.
 59

60 2. Theory

61 A Fabry-Perot Bragg grating is an optical resonator that combines the properties of a Fabry-
 62 Perot cavity and a Bragg grating. It consists of a waveguide between two partially reflective
 63 mirrors consisting of a Bragg grating. The Bragg grating provides wavelength-selective
 64 feedback, allowing only certain wavelengths to be coupled back into the waveguide and
 65 reinforcing the resonant mode. The resonant wavelength of the FPBG is determined by the
 66 cavity length and the grating period. By changing the cavity length or the refractive index of
 67 the waveguide, the resonant wavelength can be tuned. The quality factor of the resonator, which
 68 represents the energy storage and dissipation within the cavity, is determined by the reflectivity
 69 of the mirrors, the loss in the waveguide, and the coupling efficiency of the grating.

70 To extract the accurate loss of the Si_3N_4 waveguide, two methods are used to fit the
 71 experimental data. One method uses a transfer matrix method to simulate the transmission of
 72 the cavity [9], and the other method uses a fit of the quality factor Q_{load} as a function of cavity
 73 lengths [11,12].

74 2.1 ABCD transfer matrix model

75 The waveguide Bragg grating that we will focus on in this work is an optical waveguide device
 76 with a periodic variation of the refractive index along the propagation direction, as shown in
 77 Fig. 1(a). The corrugated grating on the sides of the waveguide (fishbone structure) with period
 78 Λ is patterned by electron beam lithography (EBL). Constructive interference between different
 79 reflections occurs when the optical path difference is an integral number of wavelength λ_0/n_{eff}
 80 in the waveguide, that is the period of the grating satisfy the following Bragg condition,

$$81 \quad \Lambda = \frac{m\lambda_0}{2n_{eff}}, \quad m = 1, 2, 3, \dots \quad (1)$$

82 where λ_0 is the vacuum wavelength of light, and n_{eff} is the group index of the waveguide. It
 83 includes both the average index and the index variation with wavelength. This waveguide
 84 Bragg grating can also be considered as a diffraction grating which diffracts the forward-
 85 travelling wave into a backward-traveling wave.

86 In the periodic waveguide Bragg gratings, the alternating layers with two different
 87 refractive indices can be treated as a unit cell, see Fig. 1(b). Since the optical wave is guided
 88 within the waveguide, we can consider the light to propagate only in the z direction. A general
 89 solution to the wave equation can be formed by writing:

$$90 \quad \vec{E}(z, t) = \vec{E}(z)e^{i\omega t} \quad (2)$$

91 The electric field within each layer can be expressed as a sum of a forward-traveling (+z)
 92 and a backward-travelling (-z) plane wave,

$$93 \quad \vec{E}(z) = \begin{cases} a_n e^{-ik_{1z}(z-n\Lambda)} + b_n e^{+ik_{1z}(z-n\Lambda)}, & n\Lambda - l_1 < z < n\Lambda \\ c_n e^{-ik_{2z}(z-n\Lambda+l_1)} + d_n e^{+ik_{2z}(z-n\Lambda+l_1)}, & (n-1)\Lambda < z < n\Lambda - l_1 \end{cases} \quad (3)$$

94 with $k_{1z} = \frac{n_1\omega}{c}$, $k_{2z} = \frac{n_2\omega}{c}$, where n stands for the n th period, and a_n , b_n , c_n and d_n are
 95 constants that are related by the continuity conditions at the interfaces.

96 Without loss of generality, we consider a TE-like mode. By requiring the continuity of E_x
 97 and H_y at two interfaces $z = (n-1)\Lambda$ and $z = n\Lambda - l_1$, we get $\begin{bmatrix} a \\ b \end{bmatrix} = \begin{bmatrix} A & B \\ C & D \end{bmatrix} \begin{bmatrix} c \\ d \end{bmatrix}$, where

$$98 \quad \begin{cases} A = \frac{1}{2k_{1z}}(k_{2z} + k_{1z})e^{ik_{2z}l_2} \\ B = -\frac{1}{2k_{1z}}(k_{2z} - k_{1z})e^{-ik_{2z}l_2} \\ C = -\frac{1}{2k_{1z}}(k_{2z} - k_{1z})e^{ik_{2z}l_2} \\ D = \frac{1}{2k_{1z}}(k_{2z} + k_{1z})e^{-ik_{2z}l_2} \end{cases} \quad (4)$$

99 To take the loss terms into consideration, we need to add an imaginary part to k_{1z} and k_{2z} ,

$$100 \quad k_{1z} = n_1 \times \frac{2\pi}{\lambda} - in_{1img} \times \frac{2\pi}{\lambda}$$

$$101 \quad k_{2z} = n_2 \times \frac{2\pi}{\lambda} - in_{2img} \times \frac{2\pi}{\lambda} \quad (5)$$

102 Note that $\alpha = 4\pi n_{img}/\lambda$, and we have two loss terms, the grating loss α_g and the cavity loss α_c .

103 The transfer matrix $T_i = \begin{bmatrix} A & B \\ C & D \end{bmatrix}$ is used to calculate the overall transmission T of the FBPG
 104 device, where $T = T_N T_{N-1} T_{N-2} \cdots T_2 T_1$. We further get $\begin{bmatrix} a_0 \\ b_0 \end{bmatrix} = T \begin{bmatrix} a_N \\ b_N \end{bmatrix}$. Then, the reflection and
 105 transmission coefficients of FBPG are given by $r_N = \left(\frac{b_0}{a_0}\right)_{b_N=0}$, and $t_N = \left(\frac{a_N}{a_0}\right)_{b_N=0}$.

106 2.2 Q vs L model

107 Both FPBG and micro ring resonators are types of optical resonators that rely on the
 108 constructive interference of light waves to create resonances at specific wavelengths. The main
 109 difference between FPBG and micro ring resonators is in the mechanism of resonant coupling.
 110 We take the analogy between the two resonators. Based on the model described in [11], we
 111 established a new model to extract the propagation loss in the FP cavity, and the coupling loss
 112 between the grating Bloch mode and the cavity mode.

113 We know that in the add/drop micro ring resonator, the theoretically obtainable loaded Q
 114 and intrinsic Q are,

$$115 \quad Q_{load}^{ring} \approx \frac{2\pi n_{eff} L}{\lambda} [2K + \alpha L + 2\gamma]^{-1} \quad (6)$$

$$116 \quad Q_{int}^{ring} = \frac{2\pi n_{eff} L}{\lambda} [\alpha L + 2\gamma]^{-1} \quad (7)$$

117 where K is the power coupling coefficient, α is propagation loss, L is the perimeter of the ring
 118 resonator, and γ is the excess fractional power loss of the coupler.

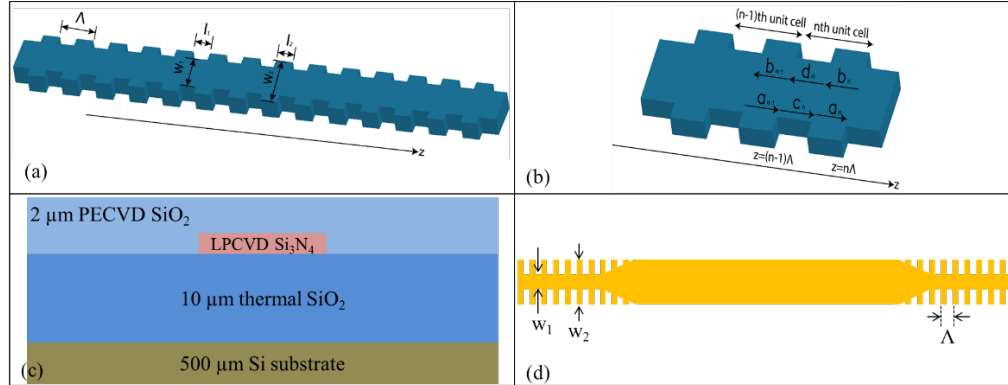
119 The FPBG resonator is analogous to an add/drop ring resonator. We can equate the BG
 120 reflectance R with $1 - K$. With the cavity length of L, and the excess power coupling loss due
 121 to mode mismatch between the grating mode and the cavity mode, we obtain the theoretical
 122 loaded Q and intrinsic Q of FPBG as,

$$123 \quad Q_{load}^{FPBG} \approx \frac{2\pi n_{eff} L}{\lambda} [2(1 - R) + \alpha L + 2\gamma]^{-1} \quad (8)$$

$$124 \quad Q_{int}^{FPBG} = \frac{2\pi n_{eff} L}{\lambda} [\alpha L + 2\gamma]^{-1} \quad (9)$$

125 By measuring the Q_{load} and fitting it as a function of cavity lengths, we can extract the
 126 propagation loss α and the coupling loss γ . Furthermore, the intrinsic Q_{int} can be calculated.

127



128

129

130

131

132

Fig. 1 (a) Schematic illustration of a typical periodic waveguide Bragg grating. (d) Complex amplitudes of the forward-travelling and backward-travelling plane waves in each layer. (c) Waveguide cross section illustration. (d) Illustration of the Fabry-Perot Bragg grating design with tapered grating.

133

3. Device design, fabrication and characterization

134

3.1 Device design

135

136

137

138

139

140

141

142

143

144

For the Fabry-Perot Bragg grating cavity, two different Si_3N_4 film thickness are chosen to be optimized in this work. The thickness is 100 nm and 300 nm separately, which is formed by low pressure chemical vapor deposition (LPCVD), as shown in Fig. 1(c). To reduce the mode mismatch between the waveguide mode and the grating Bloch mode, an adiabatic tapered grating is added between the Bragg grating and the cavity (shown in Fig.1(d)), which facilitates the adiabatic mode conversion and significantly reduces the grating-cavity coupling loss [10,13]. By simply linearly reducing the grating width, the grating loss can be reduced from 3.5 dB/cm to 0.36 dB/cm [10]. This also avoids exciting the higher order of modes in the cavity. A single grating period in this work is formed by two segments ($w_1 = 2 \mu\text{m}$, $w_2 = 4 \mu\text{m}$), see Fig. 1(d).

145

3.2 Device fabrication and characterization

146

147

148

149

150

151

152

The FPBG structure used in this paper (Fig. 1(a)) has layers of 10-um thermal SiO_2 as the bottom cladding, 100-nm or 300-nm Si_3N_4 deposited by LPCVD as the core layer, and 2-um SiO_2 deposited by plasma enhanced chemical vapor deposition (PECVD) as the top cladding. The FPBG design was patterned by a 100 keV Elionix ELS-G100 e-beam system. A maN-2400 negative e-beam resist film was coated as the mask to etch the Si_3N_4 layer with conductively coupled plasma (ICP) etching. After the deposition of the top cladding, a final thermal treatment of 12 hours at 1150 C was performed on some of the PIC chips.

153

3.3 Device characterization

154

155

156

157

158

159

160

161

162

163

A polarization maintaining tunable laser source (Keysight, 81607A) operating over a wavelength range of 1450 nm – 1640 nm was used to characterize the device, which has a narrow linewidth (0.1 pm) and a high signal to total source spontaneous emission ratio (>70 dB). A polarization maintaining single mode fiber (PM1550) with a typical mode-field diameter of 10.1 μm and a numerical aperture of 0.125 was used to carry the signal from the tunable laser source to the FPBG and out to the power meter. The coupling efficiency is around ~80% with optimized butt-coupling design [14]. The polarization of the signal entering the FPBG was controlled by a high precision fiber rotator (Thorlabs, HFR007). The fibers were butt-coupled to the PIC chip using a precision 3-axis stage (< 100 nm alignment tolerance). A power meter (Keysight, N7744A) with a dynamic range of 65 dB was used to analyze the transmitted signal.

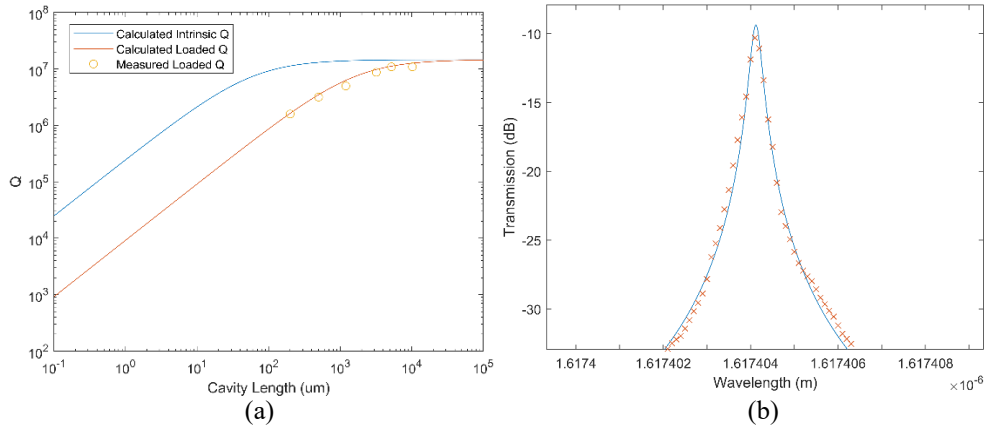
164 **4. Results and discussion**

165 **4.1 100-nm thick Si₃N₄ platform**

166 In Fig. 2, we show the highest quality factor measured in 100-nm thick Si₃N₄ device. The FPBG
 167 has a cavity width of 4 μm, and the chip was annealed under 1150 C for 12 hours. In Fig. 2(a),
 168 we plot the loaded quality value Q_{load} as a function of cavity lengths. The equation (8) is used
 169 to fit the propagation loss α and the coupling loss γ , where R is the reflectance of the Bragg
 170 grating on each side of the cavity, L is the cavity length. The intrinsic quality factor Q_{int} can be
 171 calculated by eliminating the reflectance term, R. From the fitting results, we extract the
 172 propagation loss α to be 0.017 dB/cm, and the coupling loss γ to be 0.0005 dB. The small
 173 coupling loss is due to the tapered grating design. For the cavity length of 10 mm, the loaded
 174 quality factor Q_{load} is measured to be 10.9 million, which corresponds to an intrinsic quality
 175 factor Q_{int} 14.7 million.

176 In Fig. 2(b), the transmission of the Fabry-Perot Bragg grating with 5-mm cavity length
 177 was used to fit the results by the transfer matrix method. We plot the simulation result at one
 178 of the resonance peaks with a cavity waveguide propagation loss α_c of 0.02 dB/cm, a grating
 179 propagation loss α_g of 0.25 dB/cm, and a coupling loss of 0.0005 dB. Note that α_c is the
 180 dominant factor for the Q values in the Fabry-Perot Bragg grating resonator [9].

181 The fitted results obtained by the two approaches, Q vs L model and ABCD transfer matrix
 182 model, are in good agreement.



183
 184
 185 Fig. 2 100-nm thick Si₃N₄ platform. (a) Experimental (circle) Q_{loads} , calculated Q_{load} and Q_{int} as a function of Fabry-
 186 Perot cavity lengths. (b) Experimental (crossed) resonance peak fitting by transfer matrix method.

187 To explore the effect of the waveguide core width and the annealing condition, different FPBG
 188 design and fabrication processes were performed. In Table. 1, we summarized the extracted
 189 propagation losses and coupling losses under different conditions. For a FPBG device with a
 190 2-μm wide cavity, the propagation loss is improved from 0.27 dB/cm to 0.03 dB/cm after
 191 annealed under 1150 C for 12 hours. When the width of the cavity increased to 4 μm, the
 192 propagation loss is reduced to 0.11 dB/cm, compared to 0.27 dB/cm. With the thermal
 193 treatment, the propagation loss further reduced to 0.017 dB/cm. For all the devices, the grating
 194 coupling loss is extracted to be as low as 0.001 dB/pass, which is mostly due to the introduction
 195 of a tapered grating.

196 Table. 1 100-nm Si₃N₄ platform: FPBG loss extraction under different conditions.

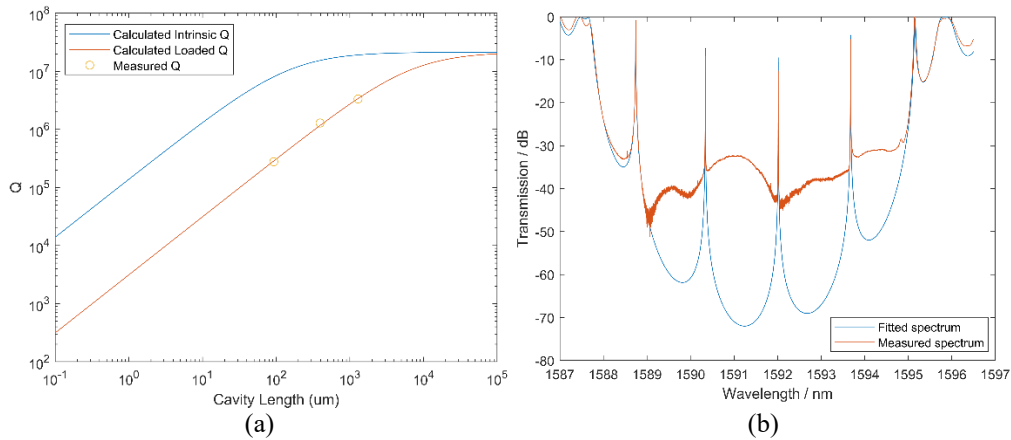
Cavity width	α	Post-SiO ₂ annealing	
		No	12 hours @1150 C
2-um	α	0.27 dB/cm	0.03 dB/cm

	γ	0.001 dB/pass	0.001 dB/pass
4-um	α	0.11 dB/cm	0.017 dB/cm
	γ	0.001 dB/pass	0.0005 dB/pass

197 **4.2 300-nm thick Si₃N₄ platform**

198 We implemented the same grating unit ($w_1 = 2 \mu\text{m}$, $w_2 = 4 \mu\text{m}$) in 300-nm thick Si₃N₄ platform
 199 as in 100-nm thick Si₃N₄ platform, while the number of grating periods was modified to obtain
 200 similar reflectance from the FPBG. To achieve low propagation loss, the chip was annealed
 201 under 1150 C for 10 hours. After measuring the transmitted spectrum of the fabricated devices
 202 and characterizing the loaded Q, both the Q vs L model and ABCD transfer matrix model were
 203 used to fit the experimental data, as shown in Fig. 3. The propagation loss extracted from the
 204 two models are 0.013 dB/cm and 0.014 dB/cm respectively, which are in good agreement. From
 205 the Q vs L model, we extracted the highest intrinsic quality factor Q_{int} to be 19.3 million.

206 Like the 100-nm thick Si₃N₄ platform, we observed the propagation loss reduction after
 207 the chip was annealed, from 0.07 dB/cm to 0.014 dB/cm.



208
209

210 Fig. 3 300-nm thick Si₃N₄ platform. (a) Experimental (circle) Q_{loads} , calculated Q_{load} and Q_{int} as a function of Fabry-
 211 Perot cavity lengths. (b) Measured transmitted spectrum fitting by ABCD transfer matrix method.

212 **4.3 Further discussion**

213 Both the bulk material loss and the surface scattering loss contribute to the propagation loss.
 214 The thermal treatment reduces bulk loss, which includes absorption loss due to specific
 215 chemical bonds and impurities, as well as losses from internal defects, such as nano- and micro-
 216 voids. Surface scattering loss is mostly due to the mode overlapping with the interfaces, which
 217 includes top, bottom, and sidewalls. The thicker and wider cavity provides a lower propagation
 218 loss, thanks to the lower overlap between the propagated mode and the interfaces of the Si₃N₄
 219 core [2,3].

220 We note that lower propagation losses are also expected on thinner Si₃N₄ platform (< 60
 221 nm) [1], as the supported mode is less confined. The delocalized mode leads to less surface
 222 scattering loss, which reduces the propagation loss significantly when the bulk material loss is
 223 minimal. However, the demonstrated high-Q resonators on thin Si₃N₄ film are mostly based on
 224 micro-ring structure. The footprint of such components is relatively large due to the limitation
 225 of critical bending radius. Since there is no bending loss concern in FPBG devices, resonators
 226 based on FPBG can be easily implemented on thin Si₃N₄ film.

227 **5. Conclusion**

228 An ultrahigh quality factor of 19.3 million for a Fabry-Perot Bragg grating resonator is
229 demonstrated. Two methods, Q vs L and the transfer matrix method, have been used to extract
230 the loss of the Si₃N₄ film. The propagation loss is as low as 0.014 dB/cm, while the coupling
231 loss between the grating mode and the cavity mode is as low as 0.0005 dB per pass. The FPBG
232 can be seamlessly integrated into a compact straight waveguide, requiring minimal additional
233 space. As a result, it serves as a vital component in the construction of advanced photonic
234 integrated circuits for various applications, enabling high-performance functionality.
235

236 **Funding.** National Science Foundation under grant 1711377, the National Aeronautics and Space Administration
237 (NASA) under grant 16-APRA 16-0064 and 21-APRA-21-0116.

238 **Acknowledgments.** We acknowledge the support of the Maryland NanoCenter and its FabLab.

239 **Disclosures.** The authors declare no conflicts of interest.

240 **Data availability.** Data underlying the results presented in this paper are not publicly available at this time but may
241 be obtained from the authors upon reasonable request.
242

243 References

- 244 1. M. W. Puckett, K. Liu, N. Chauhan, Q. Zhao, N. Jin, H. Cheng, J. Wu, R. O. Behunin, P. T. Rakich, K. D.
245 Nelson, and D. J. Blumenthal, "422 Million intrinsic quality factor planar integrated all-waveguide resonator
246 with sub-MHz linewidth," *Nat Commun* **12**, 934 (2021).
- 247 2. J. Liu, G. Huang, R. N. Wang, J. He, A. S. Raja, T. Liu, N. J. Engelsen, and T. J. Kippenberg, "High-yield,
248 wafer-scale fabrication of ultralow-loss, dispersion-engineered silicon nitride photonic circuits," *Nat*
249 *Commun* **12**, 2236 (2021).
- 250 3. X. Ji, S. Roberts, M. Corato-Zanarella, and M. Lipson, "Methods to achieve ultra-high quality factor silicon
251 nitride resonators," *APL Photonics* **6**, 071101 (2021).
- 252 4. W. Jin, Q.-F. Yang, L. Chang, B. Shen, H. Wang, M. A. Leal, L. Wu, M. Gao, A. Feshali, M. Paniccia, K. J.
253 Vahala, and J. E. Bowers, "Hertz-linewidth semiconductor lasers using CMOS-ready ultra-high-Q
254 microresonators," *Nature Photonics* **15**, 346–353 (2021).
- 255 5. X. Ji, J. K. Jang, U. D. Dave, M. Corato-Zanarella, C. Joshi, A. L. Gaeta, and M. Lipson, "Exploiting
256 Ultralow Loss Multimode Waveguides for Broadband Frequency Combs," *Laser & Photonics Reviews* **15**,
257 2000353 (2021).
- 258 6. X. Ji, F. A. S. Barbosa, S. P. Roberts, A. Dutt, J. Cardenas, Y. Okawachi, A. Bryant, A. L. Gaeta, and M.
259 Lipson, "Ultra-low-loss on-chip resonators with sub-milliwatt parametric oscillation threshold," *Optica*,
260 *OPTICA* **4**, 619–624 (2017).
- 261 7. Y. Xuan, Y. Liu, L. T. Varghese, A. J. Metcalf, X. Xue, P.-H. Wang, K. Han, J. A. Jaramillo-Villegas, A. A.
262 Noman, C. Wang, S. Kim, M. Teng, Y. J. Lee, B. Niu, L. Fan, J. Wang, D. E. Leaird, A. M. Weiner, and M.
263 Qi, "High-Q silicon nitride microresonators exhibiting low-power frequency comb initiation," *Optica*,
264 *OPTICA* **3**, 1171–1180 (2016).
- 265 8. B. Stern, X. Ji, Y. Okawachi, A. L. Gaeta, and M. Lipson, "Battery-operated integrated frequency comb
266 generator," *Nature* **562**, 401 (2018).
- 267 9. Y. Hu, Y. Zhang, P. Gatkine, J. Bland-Hawthorn, S. Veilleux, and M. Dagenais, "Characterization of Low
268 Loss Waveguides Using Bragg Gratings," *IEEE Journal of Selected Topics in Quantum Electronics* **24**, 1–8
269 (2018).
- 270 10. S. Xie, Y. Zhang, Y. Hu, S. Veilleux, and M. Dagenais, "On-Chip Fabry-Perot Bragg Grating Cavity
271 Enhanced Four-Wave Mixing," *ACS Photonics* **7**, 1009–1015 (2020).
- 272 11. O. Schwelb, "Transmission, Group Delay, and Dispersion in Single-Ring Optical Resonators and Add/Drop
273 Filters - A Tutorial Overview," *J. Lightwave Technol.*, *JLT* **22**, 1380 (2004).
- 274 12. Y. Zhang, J. Zhan, S. Veilleux, and M. Dagenais, "Silicon Nitride Fabry-Perot Bragg Grating Nanoresonator
275 with Ultrahigh Intrinsic Q," in *Conference on Lasers and Electro-Optics (2022), Paper SM4G.7* (Optica
276 Publishing Group, 2022), p. SM4G.7.
- 277 13. P. Lalanne, S. Mias, and J. P. Hugonin, "Two physical mechanisms for boosting the quality factor to cavity
278 volume ratio of photonic crystal microcavities," *Opt. Express*, *OE* **12**, 458–467 (2004).
- 279 14. T. Zhu, Y. Hu, P. Gatkine, S. Veilleux, J. Bland-Hawthorn, and M. Dagenais, "Ultrabroadband High
280 Coupling Efficiency Fiber-to-Waveguide Coupler Using Si₃N₄/SiO₂ Waveguides on Silicon," *IEEE Photonics*
281 *Journal* **8**, 1–12 (2016).
282